Simulating the sound transmission loss of complex curved panels with attached noise control materials using periodic cell wavemodes

F. Errico, G. Tufano, O. Robin, N. Guenfoud, Mohamed Ichchou, Noureddine Atalla

Simulating the sound transmission loss of complex curved panels with attached noise control materials using periodic cell wavemodes

F. Errico[a,b,*], G. Tufano[a,d], O. Robin[c], N. Guenfoud[a,d], M. Ichchou[a], N. Atalla[c]

[a] *Vibroacoustics & Complex Media Research Group, LTDS-CNRS, Ecole Centrale de Lyon, Écully, 69134, France*
[b] *Pasta-Lab, Dipartimento di Ingegneria Industriale, Universitá di Napoli Federico II, Napoli, 80125, Italy*
[c] *GAUS, Université de Sherbrooke, 2500 Boulevard de l'Université, Sherbrooke, QC, J1K 2R1, Canada*
[d] *Noise and Vibration Research Group, PMA, KU Leuven, Celestijnenlaan 300 B, B-3001, Heverlee, Belgium*

Abstract

The sound transmission loss of complex curved aircraft panels under diffuse acoustic field excitation is experimentally and numerically studied. Two different aircraft sidewall panels are considered: a thick composite sandwich panel and a thin aluminium panel with stiffening elements (stringers and frames). Both bare configuration and with attached soundproofing material are tested in laboratory conditions in coupled rooms. The numerical approach relies on a wave finite element method including modal order reduction at cell scale and an extension based on the transfer matrix method, for the inclusion of poroelastic treatments. The results obtained show that the proposed numerical scheme is efficient for predicting the sound transmission loss of such complex structures.

Keywords: Sound Transmission, Periodic Structures, Curved Composite Structures, Noise Control Materials

1. Introduction

In the aerospace industry, the requirements for lighter and stiffer structures are often strict and thus the use of composite laminates and sandwich panels for aircraft panels has become common. The reduced weight to stiffness ratio of composite sandwich structures is generally not favourable to a good vibroacoustic performance and possibly results in larger interior noise levels. At the same time, the increase of structures complexity results in a cumbersome computational cost for numerical studies extended to a large frequency bandwidth,even for small-sized models. The numerical study of optimized designs, especially for large-scale models, is thus limited.

The classic Finite Element Method (FEM) is a well-framed and accurate method that requires a finite element discretisation of the whole model, implicitly limiting its application range [1, 2, 3, 4, 5]. Alternative formulations have also been proposed to reduce the computational effort of the method [6, 7, 8].

On the other hand, Statistical Energy Analysis (SEA) is an efficient alternative, generally limited to the high frequency range. In this method, structures and substructures are studied in terms of energy exchange, strongly reducing the number of variables in the whole system [9, 10].

*Corresponding author
Email address: fabrizio.errico@ec-lyon.fr (F. Errico)

The method relies on averaged quantities and is still not preferred for acoustic problems specific of the low frequencies, even though some extensions in lower frequency bands have been proposed [11, 12]. Within the SEA framework, different works have been developed to cope with the sound transmission of composite structures [13, 14].

Analytical approaches have been proposed in the literature to deal with multi-layered panels lined with porous materials, as in [15]. Liu et al., in [16, 17, 18, 19], then proposed analytical approaches for double-walled flat and curved panels, lined with porous layers, under both acoustic sources and mean flow. Biots theory is employed and a transfer matrix equation along with appropriate boundary conditions is used to solve the system simultaneously [16, 17].

Some recent numerical alternatives have been developed to cope with a large number of engineering applications, while keeping a good compromise between accuracy, calculation time and flexibility. This is the case of the Transfer Matrix Method (TMM), which makes use of the propagating waves in infinite multilayered structures, to calculate the reflection and transmission coefficients [3, 4]. Finite size effects, that can have a large influence at low frequencies, can be included through appropriate corrections leading to a broadband accuracy of the method [20, 21, 22].

The Wave Finite Element Method (WFEM), mainly developed for periodic structures, is based on the Bloch-Floquet principle and aims to analyse the dynamics of a periodic system by imposing periodic conditions on a single repetitive cell [23, 24, 25, 26, 27, 28]. A great advantage is that the complexity of the structural shape is just addressed to the finite element modelling of a unit cell [29, 30, 31]. This approach has been applied to the analysis of the sound transmission of sandwich panels and validated under acoustic plane wave load, for flat homogenised models [32, 33], and homogeneous curved shells for fixed circumferential numbers [34]. The wave finite element method is also used to calculate SEA parameters to calculate the sound transmission of periodic structures in [35, 36].

Concerning the specific case of curved structures, alternative methods have also been presented. A mathematical model for the transmission of noise through the walls of an orthotropic cylindrical shell has been firstly proposed by Koval [37, 38, 39]. Other semi-analytic approaches, based on a receptance method, have also been suggested, in order to analyse the sound transmission of aircraft panels with stringers and ring frames, [40, 41].

Most of the cited methods are affected by limits and approximations, the frequency range of applicability of classical FEM and SEA methods being first strongly limited by computational cost or underlying hypotheses.The applicability of analytical models is often restricted to simple structural models. The TMM approach is not applicable to non-homogenised curved structures, unless the structural wavenumbers are singularly injected in the model. The previously published WFE-based approaches, in an FEM framework, are only applicable to flat and homogeneous multi-layered structures.

In this context, in this paper, a hybrid WFEM formulation is proposed, which originality stands in with the prediction of the diffuse sound transmission of complex and curved structures with attached poroelastic layers, and validated with experimental results obtained in coupled

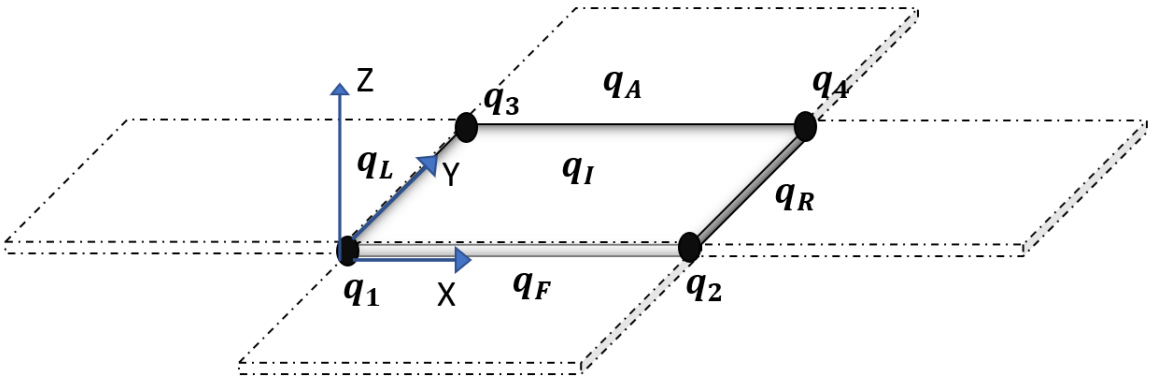

Figure 1: Example of a FE cell model with periodicity along the X-Y directions.

anechoic-reverberant rooms. The proposed formulation includes a modal order reduction at cell scale, in order to deal with heavy numerical models, and is coupled with TMM, for the inclusion of poroelastic treatments. The main aim here is to validate the method for different complex and non-homogenised cell shapes and combinations with soundproofing treatment. The main advantage stands in overcoming some of the limits of the previously described methods, aiming to deal with a wider range of case-studies: complex shapes, curvatures and attached porous layers.

2. The Numerical Approach

The wave finite element method is an FE-based method applicable to periodic structures. The first step is to perform a FE discretisation of the unit cell and extract the mass and stiffness matrices, $\mathbf{M}$ and $\mathbf{K}$ respectively. Classic meshing considerations for an appropriate wavelength description are valid as in any FE framework. With reference to Fig. 1, the dynamic stiffness equation of the segment can be written as:

$$\mathbf{D}\mathbf{q} = \mathbf{f} + \mathbf{e}, \tag{1}$$

where $\mathbf{q}$, $\mathbf{f}$ and $\mathbf{e}$ are the vectors of nodal degrees of freedom (DoFs), internal and external forces, respectively; $\mathbf{D}$ is the dynamic stiffness matrix. For periodic structures, assuming time and space harmonic excitation, the periodicity conditions are translated in a magnitude and phase link among each point belonging to the periodic pattern, based on complex propagating constants for each elastic wave. Displacements and forces at any point of the cell can thus be connected to the ones of a limited subset, exploiting periodic links, as follows:

$$\mathbf{q}_A = \mathbf{I}\lambda_Y \mathbf{q}_F; \qquad \mathbf{q}_R = \mathbf{I}\lambda_X \mathbf{q}_L; \qquad \mathbf{q}_2 = \mathbf{I}\lambda_X \mathbf{q}_1; \qquad \mathbf{q}_3 = \mathbf{I}\lambda_Y \mathbf{q}_1; \qquad \mathbf{q}_4 = \mathbf{I}\lambda_X\lambda_Y \mathbf{q}_1; \tag{2}$$

with

$$\lambda_X = \mathrm{e}^{-\mathrm{i}k_X L_X}, \qquad \lambda_Y = \mathrm{e}^{-\mathrm{i}k_Y L_Y}, \tag{3}$$

where k_X and k_Y are wavenumbers of the propagating wave in the periodicity directions X and Y, while L_X and L_Y represent the cell lengths along the same directions, respectively; $\mathbf{I}$ is the identity

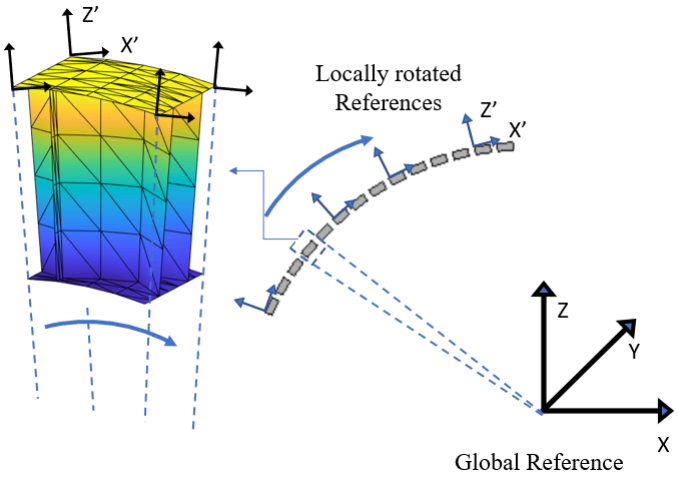

Figure 2: Example of a FE cell curved rotating the local nodal references.

matrix. Assembling in a block-diagonal form the periodicity condition matrices, as in Eq. 2, a periodicity matrix $\mathbf{\Lambda}$ can be used to link the total displacements and forces vectors to a reduced subset of degrees of freedom. Pre-multiplying Eq.1 by $\mathbf{\Lambda}^H$, where H stands for the hermitian operator, the dynamic stiffness matrix of the reduced model ($\mathbf{D}_S$) is given by Eq. 4.

$$\mathbf{D}_S = \mathbf{\Lambda}^{\mathrm{H}}[\mathbf{K} - \omega^2\mathbf{M}]\mathbf{\Lambda}. \tag{4}$$

Given the equilibrium of the internal forces between consecutive cells, only potential external forces are considered [25].

The problem in Eq. 4 represents a three-parametric eigenproblem in ω, λ_X and λ_Y, that can be solved by imposing two of the variables at each step [25]. In this way, the propagating wavemodes and the corresponding constants of propagation can be derived.

The present work being focused on curved structures, the local nodal coordinate system, in the FE mesh of the unit cell, can be rotated to simulate the desired curvature. This way, imposing the periodicity conditions as shown in Eq. 3, the wave propagation is automatically analysed along the curved local path. To model the curved cell, as in Fig. 2, a rotational matrix is assembled in a block diagonal matrix, **Rot**, [42, 43]. Hence, the mass and stiffness matrices of the singly curved periodic structure can be calculated as in Eq. 5.

$$\mathbf{M}_{\mathrm{curv}} = \mathbf{Rot}^{\mathrm{T}}\mathbf{MRot}; \qquad \mathbf{K}_{\mathrm{curv}} = \mathbf{Rot}^{\mathrm{T}}\mathbf{KRot}, \tag{5}$$

where the subscript curv refers to the mass and stiffness matrices of the cell being simulated as curved. The waves analysed along the locally curved reference are circumferential waves [26]. Forcing wavenumbers, imposed after Eq. 5, represent helical waves, in general.

2.1. Modal Order Reduction at cell scale

The use of modal reduction is highly suggested for fine meshes. In these cases, the internal degrees of freedom, are substituted by the modal participation factors to achieve a significant reduction of the number of inner DOFs [44]. The displacement vector $\mathbf{q}$ defined in Eq. 1, is here

partitioned in $[\mathbf{q}_J, \mathbf{q}_B]$. The vector $\mathbf{q}_B$ represents the degrees of freedom of the nodes belonging to subset on the borders of the structure in both X, Y and Z. On the contrary, $\mathbf{q}_J$ represents the nodes belonging to the inner part of the cell. This way, Eq. 1 takes the form of Eq. 6.

$$\left(\begin{bmatrix} \mathbf{K}_{BB} & \mathbf{K}_{BJ} \\ \mathbf{K}_{JB} & \mathbf{K}_{JJ} \end{bmatrix} - \omega^2 \begin{bmatrix} \mathbf{M}_{BB} & \mathbf{M}_{BJ} \\ \mathbf{M}_{JB} & \mathbf{M}_{JJ} \end{bmatrix} \right) \begin{bmatrix} \mathbf{q}_B \\ \mathbf{q}_J \end{bmatrix} = \begin{bmatrix} \mathbf{f}_B \\ \mathbf{f}_J \end{bmatrix}, \tag{6}$$

where $\mathbf{f}_J$ is null, since no load is applied on this subset of nodes. The displacements vector can be expressed as in Eq. 7, using a reduced basis that involves the static boundary modes $\mathbf{\Psi}_B$ and component modes $\mathbf{\Psi}_C$:

$$\begin{bmatrix} \mathbf{q}_B \\ \mathbf{q}_J \end{bmatrix} = \mathbf{G} \begin{bmatrix} \mathbf{q}_B \\ \mathbf{P}_J \end{bmatrix}; \qquad \mathbf{G} = \begin{bmatrix} \mathbf{I} & \mathbf{0} \\ \mathbf{\Psi}_B & \mathbf{\Psi}_C \end{bmatrix} \tag{7}$$

where $\mathbf{P}_J$ is the set of retained modal participation factors and $\mathbf{G}$ is the projection matrix for the new basis. The static boundary modes $\mathbf{\Psi}_B$ and component modes $\mathbf{\Psi}_C$ can be derived as in a Craig-Bampton (CB) framework (Eq. 8).

$$\mathbf{\Psi}_B = \mathbf{K}_{JJ}^{-1}\mathbf{K}_{JB}; \qquad (\mathbf{K}_{JJ} - \omega^2\mathbf{M}_{JJ})\mathbf{\Psi}_C = \mathbf{0}. \tag{8}$$

So, the displacements inside a unit-cell can be expanded on a subset of stationary modes [44]. Finally the stiffness and mass matrices can be written in the reduced set of coordinates using the projection matrix $\mathbf{G}$ defined in Eq. 7:

$$\begin{aligned} \mathbf{M}_{\text{Cond}} &= \mathbf{G}^{\text{T}}\mathbf{M}\mathbf{G}, \\ \mathbf{K}_{\text{Cond}} &= \mathbf{G}^{\text{T}}\mathbf{K}\mathbf{G}, \end{aligned} \tag{9}$$

where the subscript cond refers to the mass and stiffness matrices of the cell being condensed. The set of retained modal participation factors, $\mathbf{P}_J$, can be then statically condensed at each frequency step.

2.2. The Sound Transmission Problem

Lets assume a structural model made of two external skins, i.e. a sandwich plate or a ribbed panel. When an acoustic plane wave of amplitude p_I impinges on one face of the infinite structure, it vibrates and sound pressure waves are transmitted and reflected in the fluid adjacent to the excited and radiating surfaces of the structures. Subscripts *exc* and *rad* are now used to identify the subset of DoF, quantities and domains connected to the excited and radiating parts of the structure, respectively. The degrees of freedom that do not belong to these two subsets, are identified using the subscript In.

Taking the X-Y plane as a reference plane (Fig. 1), an acoustic plane wave can be defined, on the surface of the cell, omitting the time harmonic dependence, as:

$$p(X, Y, Z, \omega) = p_I \mathrm{e}^{-\mathrm{i}(k_X X + k_Y Y - k_{Z,exc} Z)}, \tag{10}$$

where the trace wavenumber components k_X and k_Y are defined following the angles of incidence (θ and ϕ; see Fig. 3) and the acoustic wavenumber (k_0), as in Eq. 11.

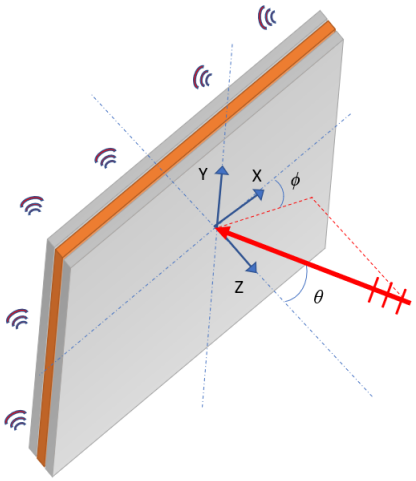

Figure 3: Incident acoustic wave on the X-Y plane of the structure.

$$k_X = k_{exc}\sin\theta\cos\phi; \qquad k_Y = k_{exc}\sin\theta\sin\phi; \qquad k_{Z,exc} = \sqrt{k_{exc}^2 - k_X^2 - k_Y^2}. \tag{11}$$

The wavenumber components k_X and k_Y are conserved along the structure, if we assume homogenised layers. For non-homogenised layers, since the numerical procedure includes periodic links (Eq. 2), the multiple harmonics resulting from the periodicty of the structural system are automatically included in the response of the radiating surface for each forcing wave of wavenumbers k_X and k_Y. The k_Z component can vary with the nature of the fluid; it the case here studied both domains are made of air so k_{exc} and k_{rad} coincide and are equal to k_0 $(= \omega/c_0)$.

From continuity of the normal particle velocity on the excited and radiating surfaces, the dynamic stiffness of the fluids can be derived.

$$D_{f,exc} = \frac{-\mathrm{i}\rho_{exc}\omega^2}{k_{Z,exc}}; \qquad D_{f,rad} = \frac{-\mathrm{i}\rho_{rad}\omega^2}{k_{Z,rad}}, \tag{12}$$

where ρ_{exc} and ρ_{rad} are the fluid densities in the two domains and $D_{f,exc}$ and $D_{f,rad}$ the dynamic stiffness of the fluid in the incident and radiating domains, respectively, linking the displacements to the sound pressure amplitude in the two domains. It is worth clarify that the present procedure is applicable also to curved structures. The curvature simulation exploited in Eq. 5, leads to a local wavemode reference. The wavenumbers k_X and k_Y become the local circumferential and axial wavenumbers and thus Eq. 10 is representative of an helical wave: the load is decomposed in a local reference which is coherent with the simulated curved structure. In this way, the load must not be decomposed into spherical waves as in [37, 14, 13].

The load imposed on the plate, by the forcing plane wave (Eq. 10), can be simply lumped on the wetted (excited) nodes of the finite element model. This way, the force vector of the subset of nodal degrees of freedom as in Eq. 2, can be partitioned as in Eq. 13:

$$\mathbf{e}^r_{exc} = \mathbf{S}\cdot(\mathbf{p}_I + \mathbf{p}_R); \qquad \mathbf{e}^r_{In} = \mathbf{0}; \qquad \mathbf{e}^r_{rad} = \mathbf{S}\cdot\mathbf{p}_T, \tag{13}$$

where $\mathbf{S}$ is the vector of the free nodal areas of each excited node and $\mathbf{p}_I$, $\mathbf{p}_R$ and $\mathbf{p}_T$ are the nodal pressure vectors representing the incoming, reflected and transmitted sound wave amplitudes,

respectively. The dynamic stiffness matrix can be rearranged in the same way as the forces in Eq. 13, condensing all the non-excited nodes and resulting in $\mathbf{D}_S^c$. Including the relations of Eq. 12, the dynamic problem results in:

$$\left[\mathbf{D}_S^c\right] \begin{bmatrix} \mathbf{p}_I - \mathbf{p}_R \\ \mathbf{p}_T \end{bmatrix} = \begin{bmatrix} \mathbf{S} \cdot D_{f,exc} \cdot (\mathbf{p}_I + \mathbf{p}_R) \\ \mathbf{S} \cdot D_{f,rad} \cdot (\mathbf{p}_T) \end{bmatrix}. \tag{14}$$

The algebraic system in Eq. 14 can be solved in $\mathbf{p}_R$ and $\mathbf{p}_T$ obtaining the sound power transmission coefficient τ.

$$\tau(\theta, \phi) = \frac{(k_{Z,exc}/\rho_{exc})\mathbf{S}|\mathbf{p}_T^2|}{(k_{Z,rad}/\rho_{rad})\mathbf{S}|\mathbf{p}_I^2|}. \tag{15}$$

Finite size effects can be included through correction factors in order to increase the accuracy at low frequencies. While a formal and accurate spatial windowing approach is presented in [22], the computational cost associated with this step might be high. Asymptotic formulas as in [21] are used to reduce the computational cost, when homogeneous structures are analysed, even if these lead to a loss of accuracy with respect to proper windowing at low frequency.

To simulate the sound transmission loss under a diffuse acoustic field, an integration of the transmission coefficient is performed between zero and the maximum angle of incidence θ_{max}, as in Eq. 16.

$$\tau_d(\omega) = \frac{1}{\pi} \int_0^{2\pi} \int_0^{\theta_{max}} \tau(\theta, \phi) \sin\theta \cos\theta \mathrm{d}\theta \mathrm{d}\phi. \tag{16}$$

Some issues in numerically evaluating this integral might arise when the values of θ_{max} approach 90 degrees [45]. The sound transmission loss, TL, under a diffuse acoustic field is then computed as:

$$\mathrm{TL}(\omega) = -10 \log_{10}(\tau_d(\omega)). \tag{17}$$

2.3. A TMM-based extension for attached porous layers

While some works have been developed directly to model and analyse porous materials using WFE [46, 47], here a simple approach is proposed to couple the present approach with the modelling of infinite porous layers using TMM. Lets consider two laterally infinite sections, as in Fig. 4, where the first one represents a potential periodic structure analysed using WFE-based approach and the second one a porous material attached to the previous layer. By considering the continuity of the velocities at the interface between the structural cell and the porous layer (plane 2 in Fig. 4), the incoming pressure in the second layer can be derived using the surface impedance of the porous layer itself, assuming the surface to be fully covered by the subsequent one. First, by solving Eq. 14 and substituting p_T in Eq. 12, the averaged vibrational velocity, on the radiating side of the first layer, is calculated. Then, once the nature of the second layer is established, the surface impedance (Z_S) can be derived and p_2 calculated, using the equivalent fluid layer theory [3, 48]. In addition, no interaction between nodes on a face or cross face of the porous layer is assumed [3, 48]. Finally, the sound pressure in the radiating side (plane 3 in Fig. 4) is evaluated using the classic Transfer Matrix Method, as in Eq. 18.

$$\begin{bmatrix} p_2 \\ v_2 \end{bmatrix} = \begin{bmatrix} \cos k_Z h_p & \mathrm{i} Z_c \sin k_Z h_p \\ \mathrm{i} Z_c^{-1} \sin k_Z h_p & \cos k_Z h_p \end{bmatrix} \begin{bmatrix} p_3 \\ v_3 \end{bmatrix}, \tag{18}$$

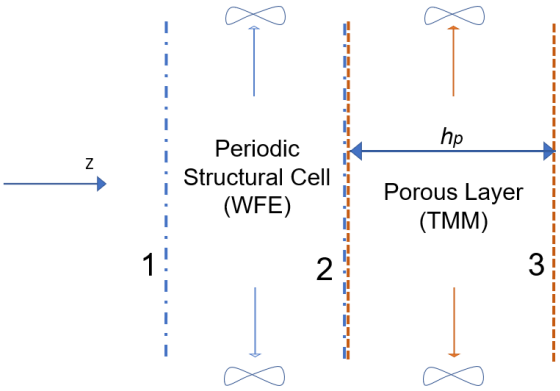

Figure 4: Illustration of the two laterally infinite sections representing the structural layer and the porous one.

where h_p represents the thickness of the porous layer, Z_c its characteristic impedance and the subscripts 2 and 3 are used to identify the sound pressure and the particle velocity at interface/plane 2 and 3 (Fig. 4), respectively. The transmission coefficient of the cell including the porous treatment equals the product of the transmission coefficients of the single stations $1-2$ and $2-3$ (see Fig. 4).

This extension, while exact and immediate for homogenised structures, it is an approximation for complex-shaped cells. A proper coupling for each structural part exposed or in contact with the subsequent fluid layer is not performed, but, as will be shown in the following sections, this approximation still provides accurate and predictive results in the case of complex shaped cells.

3. Experimental Set-Up

3.1. Transmission Loss Measurements

The measurements were performed in the coupled reverberant-anechoic rooms at Groupe d' acoustique de Université de Sherbrooke, following closely the standard (ISO 15186-1: 2000), as in [49, 50] (see Fig. 5). The reverberant room has dimensions 7.5 x 6.2 x 3 m^3 with an averaged reverberation time (T_{60}) of 5.5 s in the frequency band [50-1000] Hz (Schroeder frequency $= 2000\sqrt{T_{60}/V} \approx 400$ Hz; [51]). The acoustic excitation is generated using loudspeaker installed close to a corner of the room, with a white noise input from 50 to 5000 Hz.

The transmitted sound power is estimated using a sound intensity probe in the receiving semi-anechoic room: a Bruel & Kjaer sound intensity probe composed of two half-inch microphones and a 12 mm spacer was used. In a diffuse sound field, the incident sound power is related to the spatially-averaged mean quadratic sound pressure. This quantity can be obtained either using several fixed microphones in the reverberant room, or a single moving (traverse) microphone which is used here using a rotating boom as in Fig. 5. The sound transmission loss (TL), now defined at Eq. 17, is finally calculated, assuming that the excited and radiating surfaces are the same, as:

$$\mathrm{TL} = L_p - L_i - 6, \tag{19}$$

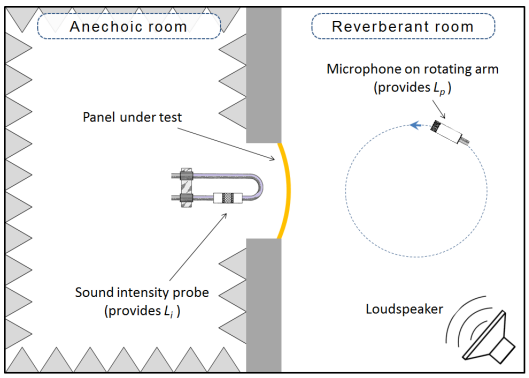

Figure 5: Illustration of the test facility with coupled reverberant-anechoic rooms. TL measurement following pressure-intensity standard.

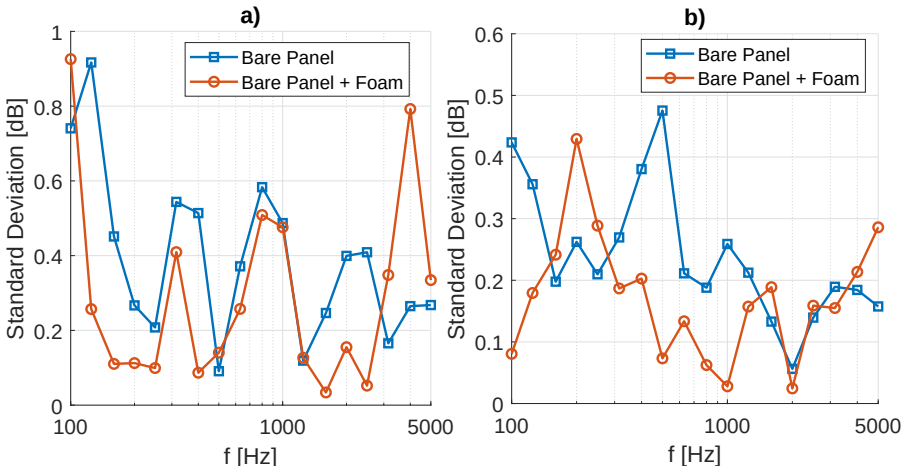

Figure 6: Standard deviation of the whole set of TL measurements following pressure-intensity standard. a) Composite Panel; b) Ribbed Panel

where L_p is the average pressure level measured in the reverberant room, L_i the average sound intensity level over the surface of the test-panels in the semi-anechoic room, while the -6 factor arises from reference values in dB conversion [45].

The tests have been performed multiple times,so as to evaluate mesaurement dispersion, and the curves presented in Fig. 8 and 10 represent a global average, in third octave bands. The standard deviation of the sound transmission loss, for the two tested panels, is reported in Fig. 6.

3.2. Tested Panels

A thick sandwich composite panel and a thin aluminium stiffened with frames and stringers are considered (Fig. 7). The composite panel has dimensions 1.54 m x 1.62 m, with a 0.94 m radius of curvature. The ribbed panel has dimensions 1.45 m x 1.70 m, with a 1.30 m radius of curvature. For each of the two panels, two different configurations are tested and numerically simulated: a bare configuration and one with a 5cm-thick melamine layer attached (see Fig. 7). The material and property data for the sandwich composite panel are provided in Table 1; the physical properties of the melamine foam are given in Table 2; the geometrical parameters for the ribbed aluminium panel are in Table 3, while the material is aluminium for all its substructures.

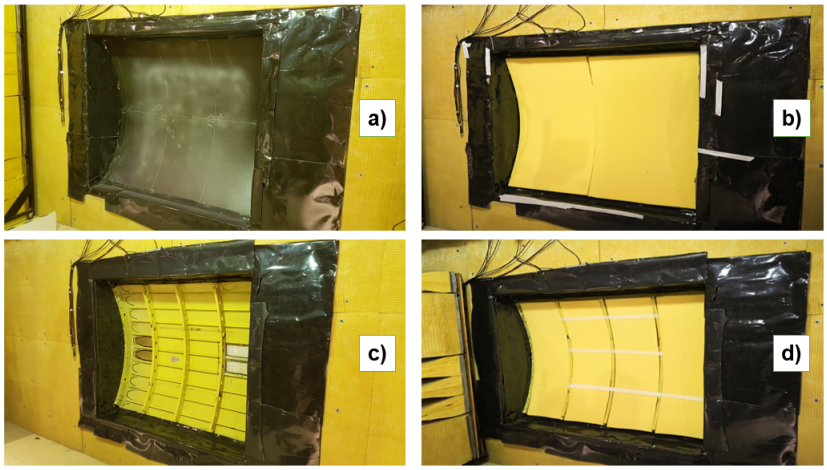

Figure 7: A view, from the semi-anechoic chamber, of the two test panels mounted in the linking window. Sandwich curved panel configurations: a) bare; b) with attached porous layers. Ribbed fuselage panel configurations: c) bare; d) with attached porous layers.

Table 1: Material properties for the thick curved composite sandwich panel.

	Skins	Core
E_1 (GPa)	46.0	0.01 x 10^{-3}
E_3 (GPa)	46.0	0.179
$G_{1,2}$ (GPa)	17.7	1.0 x 10^{-3}
$G_{1,3}$ (GPa)	17.7	26.0 x 10^{-3}
$G_{2,3}$ (GPa)	17.7	56.0 x 10^{-3}
$\nu_{1,2}$	0.3	0.45
$\nu_{1,3}$	0.3	0.01
ρ (kg/m^3)	1570	64
h (mm)	0.98	25.5

Table 2: Physical properties for the porous layers attached to the panels.

Thickness	Open porosity	Flow resistivity	Tortuosity	Viscous length	Thermal length
5 cm	0.99	7920 [Nm^{-4}s]	1.02	132 [μm]	149 [μm]

Table 3: Geometrical parameters of the ribbed fuselage panel.

	Frames	Stringers	Skin
Thickness (mm)	1.8	1.2	1.2
Height (mm)	72	28	
Spacing (mm)	40.6	15.2	

A double wall system links the rooms with a 2.44 m x 1.63 m test window, decoupled by a 12.7 mm air gap. Both panels were mounted in the test window using frames of adapted sizes, that were made of plywood with acoustic sealant made of neoprene adhesive and silicone. Only the panels skin was actually clamped over approximately 20 mm in the mounting frame (stiffeners of the aluminium panel were thus not clamped). The frames and surrounding surfaces were finally covered with a flexible decoupled barrier material composed of an open-cell foam and a heavy PVC layer. Great care was used in mounting to avoid leakage and excellent repeatability of the experiments was observed.

4. Numerical Results and Validation

4.1. Thick Sandwich Panel

First, the numerical results obtained with the presented method are compared with the measurements of the sound transmission for the curved composite sandwich panel. The unit cell is modelled using 20 solid elements (ANSYS SOLID45) through the thickness of the plate and using Eq. 5 to simulate the curvature. The porous layer is simulated using an equivalent fluid model [3].

The results in Fig. 8 show that, above the 400 Hz third octave, the numerical and experimental results are in agreement. The TMM-based extension for porous layers, described in Section 2, is here exact and gives excellent predictive results. Some discrepancies are present below 400 Hz and are attributable to a lack of accuracy of the measurements below the Schroeder frequency and to the way finite-size affects are accounted in the model. Being below the ring frequency region ($\approx$ 500 Hz), a strong stiffness of the shell, in the circumferential direction increases the sound transmission loss in that frequency band. The averaged contribution for all the integration angles of a diffuse acoustic field, induces an horizontal trend of the TL curves versus frequency, as observed in the literature [37, 13].

A high level of damping is observed in the experimental TL curves (Fig. 8), since both the ring frequency ($\approx$ 500 Hz; numerically calculated from dispersion curves; Eq. 4) and the acoustic coincidence ($\approx$ 1.5 kHz; calculated from experimental dispersion curves) are characterised by very smooth dips. The structural damping is 3% in the whole frequency band, to simulate the increased damping added by the installation in the test window, leading to a good agreement of the numerical and experimental curves.

4.2. Ribbed Fuselage Panel

Next, the sound transmission for a curved and ribbed fuselage panel (Fig. 7 (c) and (d)), is measured and compared to the presented model. The averaged TL curves, in third octave bands, are presented in Fig. 10.

A numerical simulation is performed using the method presented in Section 2. The unit cell is illustrated in Fig. 9; shell elements (ANSYS SHELL181) are used for all structural parts, while joints and connections are not included in the model. In the real model, the stringer passes through

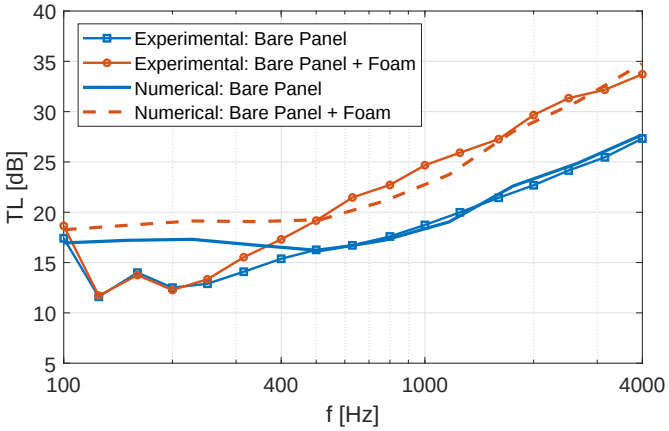

Figure 8: The Transmission Loss of a thick curved sandwich panel under diffuse acoustic field excitation. A comparison of the numerical results in log-space with measurements in third octave bands.

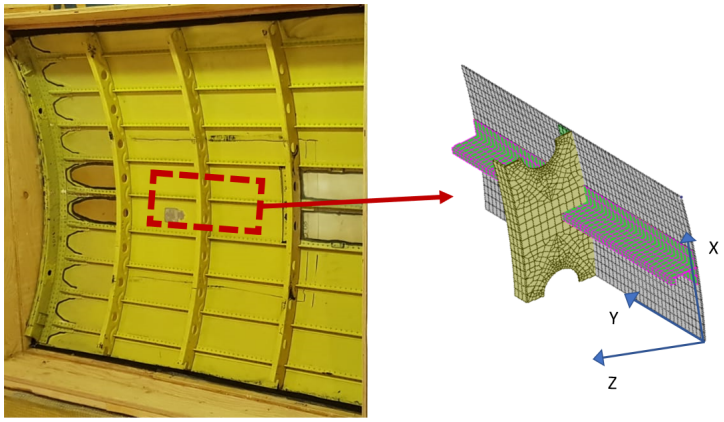

Figure 9: The unit cell used for the WFE simulation. The cell has global sizes given by the spacing of frames and stringers (Table 3).

a small hole in the frame; this is omitted in the cell model since not considered relevant for a sound radiation problem. In addition, the real panel is not perfectly periodic: some bays between the two last frames (on the left side, Fig. 7) are not coincident to the other ones in the whole panel, while the two frames at the lateral borders of the panel do not have the same geometry and size of the ones in the middle. Differences between the real structure and the ideally periodic model are thus present.

The modelled periodic cell has almost $2.9 \cdot 10^4$ degrees of freedom; the modal order reduction reduces this number to less than 4000. More than 10 elements per wavelength are used to guarantee mesh convergence for the sound transmission up to 3 kHz. This was a trade-off choice to guarantee accurate results and keep a relatively low computational cost. For this reason the numerical results are plotted just up to this frequency and not before 200 Hz, being the measured data not reliable below 400 Hz.

In Fig. 10, a good agreement with the numerical method is observed in the 300 Hz - 2500 Hz frequency range. Both for the bare configuration (Fig. 7 (c)) and the one with attached

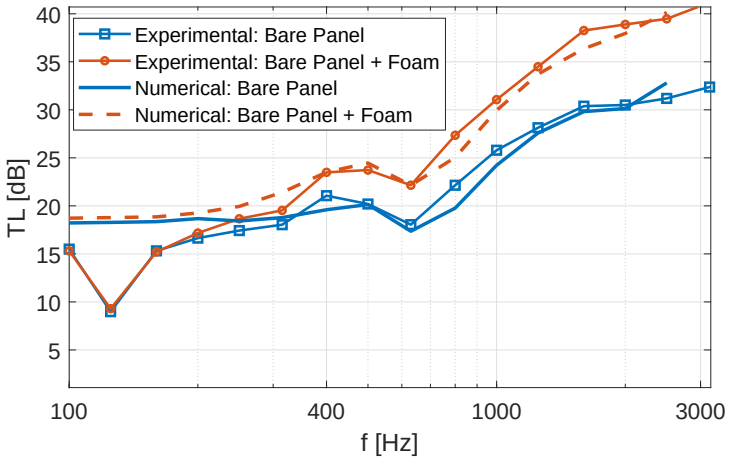

Figure 10: The Transmission Loss of the ribbed fuselage panel for a diffuse acoustic load. A comparison of the numerical results with measurements in third octave bands.

soundproofing material (Fig. 7 (d)), the numerical TL curves closely follows the experiments. The ring frequency ($\approx$ 670 Hz; [40]) gives a dip in the transmission loss, which is well described by the simulation, proving that the curvature simulation presented in Eq. 5 is still applicable even for large cell periods. Thus, unless small curvatures must be simulated, the periodic cell can be modelled as flat and Eq. 5 applied to simulate the desired curved shape.

Using the approach described in subsection 2.3 a proper fluid-structure coupling at cell scale is not performed. In addition, the air-gap between the radiating skins of the panel, between the fuselage bays, and the porous layer, have not been modelled. Considering the approximations regarding the handling of the sound package and the size effect, the discrepancies between the real structure and the model, the results observed in the test-case with the attached melamine layer, are accurate enough.

5. Concluding Remarks

A wave-based method involving an FE-modelled unit cell of a periodic structure, is validated using experimental tests on two complex curved test-panels: a thick sandwich composite panel and a doubly-ribbed aluminium one. The tests are performed in a facility equipped with semi-anechoic-reverberant coupled rooms. The transmitted power is estimated using a sound intensity probe in the receiving semi-anechoic room, while the incident power is obtained by the averaged sound pressure level in the source room measured using a rotating boom microphone, following closely the standard ISO 15186.

The measured sound transmission loss are compared to the present numerical approach in two different configurations per test-case: bare configuration and with an attached noise control material. The method involves the use of periodic conditions on a unit-cell, modelled with finite elements, and, for large number of degrees of freedom, a modal order reduction performed to cell scale. The structure-borne radiation is described using continuity of normal displacements at the

interface with the excited and radiating fluid domains. Equivalent nodal forces are expressed by means of the dynamic stiffness of the fluid. A simple approximation to simulate the coupling with multiple layers of different nature, as the case where the porous layers are attached to the structural model, is developed in a transfer matrix framework. The curvatures of the panel are imposed by manipulating the mass and stiffness matrices of the cell modelled as flat. The final structural response is computed integrating the single response to a set of forcing circumferential and axial waves (helical wavefields).

The ring frequency and acoustic coincidences are efficiently estimated numerically, in all the test-cases analysed. The sound transmission losses are validated for all the configurations tested, above the Schroeder frequency of the room.

Acknowledgments

This project has received funding from the European Unions Horizon 2020 research and innovation programme under the Marie Sklodowska-Curie grant agreement No. 675441. Professors Sergio De Rosa and Francesco Franco are acknowledged for the fruitful discussions. Patrick Levesque is acknowledged for the installations in the TL suite.

References

[1] F. Franco, S. De Rosa, E. Ciappi, Numerical approximations on the predictive responses of plates under stochastic and convective loads, Journal of Fluids and Structures 42 (2013) 296–312. doi:/10.1016/j.jfluidstructs.2013.06.006.

[2] S. Hambric, Y. Hwang, W. Bonness, Vibrations of plates with clamped and free edges excited by low-speed turbulent boundary layer flow, Journal of Fluids and Structures 19 (1) (2004) 93–110. doi:/10.1016/j.jfluidstructs.2003.09.002.

[3] J. Allard, N. Atalla, Propagation of sound in porous media: Modelling sound absorbing materials, John Wiley & Sonsdoi:/10.1002/9780470747339.

[4] N. Atalla, Modelling the sound transmission through complex structures with attached noise control materials, Wave Motion 51 (2014) 650–663. doi:/10.1016/j.wavemoti.2013.11.001.

[5] L. Barisciano Jr, Broadband transmission loss due to reverberant excitation, NASA/CR-1999-209687, Langley Research Center, Hampton, Virginia.

[6] S. De Rosa, F. Franco, A scaling procedure for the response of an isolated system with high modal overlap factor, Mechanical Systems and Signal Processing 22 (2008) 1549–1565. doi:/10.1016/j.ymssp.2008.01.007.

[7] M. Ichchou, B. Hiverniau, B. Troclet, Equivalent rain on the roof loads for random spatially correlated excitations in the mid frequency range, Journal of Sound and Vibration 322 (2009) 926–940. doi:/10.1016/j.jsv.2008.11.050.

[8] T. Courtois, C. Bertolini, J. Ochs, A procedure for efficient trimmed body fe simulations, based on a transfer admittance model of the sound package, SAE Int. J. Passeng. Cars Mech. Syst. 3 (2010) 1–13. doi:/10.4271/2010-01-1405.

[9] R. Lyon, R. DeJong, M.Heckl, Theory and application of statistical energy analysis, second edition, The Journal of the Acoustical Society of America 98 (6) (1995) 3021–3021. doi:/10.1121/1.413875.

[10] M. Crocker, A. Price, Sound transmission using statistical energy analysis, Journal of Sound and Vibration 9 (3) (1969) 469–486. doi:/10.1016/0022-460X(69)90185-0.

[11] A. Le Bot, V. Cotoni, Validity diagrams of statistical energy analysis, Journal of Sound and Vibration 329 (2) (2010) 221–235. doi:https://doi.org/10.1016/j.jsv.2009.09.008.

[12] F. Fahy, Statistical energy analysis: a critical overview, A.J. Keane, W.G. Price (Eds.), Statistical Energy Analysis: An Overview, with Applications in Structural Dynamics, Cambridge University Press, Cambridge, 1997.

[13] S. Ghinet, N. Atalla, H. Osman, The transmission loss of curved laminates and sandwich composite panels, J. Acoust. Soc. Am. 118 (2) (2005) 774–790. doi:/10.1121/1.1932212.

[14] S. Ghinet, N. Atalla, H. Osman, Diffuse field transmission into infinite sandwich composite and laminate composite cylinders, Journal of Sound and Vibration 289 (2006) 745–778. doi:/10.1016/j.jsv.2005.02.028.

[15] J. Bolton, N.-M. Shiau, Y. Kang, Sound transmission through multi-panel structures lined with elastic porous materials, Journal of Sound and Vibration 191 (3) (1996) 317 – 347. doi:https://doi.org/10.1006/jsvi.1996.0125.
URL http://www.sciencedirect.com/science/article/pii/S0022460X9690125X

[16] Y. Liu, C. Daudin, Analytical modelling of sound transmission through finite clamped double-wall sandwich panels lined with poroelastic materials, Composite Structures 172 (2017) 359 – 373. doi:https://doi.org/10.1016/j.compstruct.2017.03.024.
URL http://www.sciencedirect.com/science/article/pii/S0263822316326204

[17] Y. Liu, C. He, Diffuse field sound transmission through sandwich composite cylindrical shells with poroelastic core and external mean flow, Composite Structures 135 (2016) 383 – 396. doi:https://doi.org/10.1016/j.compstruct.2015.09.025.
URL http://www.sciencedirect.com/science/article/pii/S0263822315008612

[18] J. Zhou, A. Bhaskar, X. Zhang, The effect of external mean flow on sound transmission through double-walled cylindrical shells lined with poroelastic material, Journal of Sound and Vibration 333 (7) (2014) 1972 – 1990. doi:https://doi.org/10.1016/j.jsv.2013.11.038.
URL http://www.sciencedirect.com/science/article/pii/S0022460X13009929

[19] Y. Liu, A. Sebastian, Effects of external and gap mean flows on sound transmission through a double-wall sandwich panel, Journal of Sound and Vibration 344 (2015) 399 – 415. doi:https://doi.org/10.1016/j.jsv.2015.01.040.
URL http://www.sciencedirect.com/science/article/pii/S0022460X15000863

[20] D. Rhazi, N. Atalla, A simple method to account for finite size effects in the transfer matrix method, J. Acoust. Soc. Am. 127 (2) (2010) EL30–EL36. doi:/10.1121/1.3280237.

[21] F. Leppington, E. Broadbent, K. Heron, The acoustic radiation efficiency from rectangular plates, Proc. R. Soc. 382 (1982) 245–271. doi:/10.1098/rspa.1982.0100.

[22] M. Villot, C. Guigou, L. Gagliardini, Predicting the acoustical radiation of finite size multi-layered structures by applying spatial windowing on infinite structures, Journal of Sound and Vibration 245 (3) (2001) 433–455. doi:/10.1006/jsvi.2001.3592.

[23] L. Brillouin, Wave Propagation in Periodic Structures: Electric Filters and Crystal Lattices, 2nd edition Dover Publications, Mineola, New York, 1953. doi:10.1016/S0031-8914(53)80099-6.

[24] D. Mead, Wave propagation in continuous periodic structures: research contributions from southampton, Journal of Sound and Vibration 190 (3) (1996) 495–524. doi:/10.1006/jsvi.1996.0076.

[25] E. Manconi, B. R. Mace, Modelling wave propagation in two dimensional structures using finite element analysis, Journal of Sound and Vibration 318(45) (2008) 884–902. doi:/10.1016/j.jsv.2008.04.039.

[26] F. Errico, M. Ichchou, S. De Rosa, O. Bareille, F. Franco, The modelling of the flow-induced vibrations of periodic flat and axial-symmetric structures with a wave-based method, Journal of Sound and Vibration 424 (2018) 32–47. doi:/10.1016/j.jsv.2018.03.012.

[27] J. M. Renno, B. R. Mace, Calculating the forced response of cylinders and cylindrical shells using the wave and finite element method, Journal of Sound and Vibration 333 (21) (2014) 5340–5355. doi:/10.1016/j.jsv.2014.04.042.

[28] J. M. Renno, B. R. Mace, Vibration modelling of structural networks using a hybrid finite element/wave and finite element approach, Wave Motion 51 (4) (2014) 566–580. doi:/10.1016/j.wavemoti.2013.09.001.

[29] E. Manconi, B. R. Mace, Wave characterization of cylindrical and curved panels using a finite element method, The Journal of the Acoustical Society of America 125 (1) (2009) 154–163. doi:/10.1121/1.3021418.

[30] E. Manconi, B. R. Mace, R. Garziera, The loss-factor of pre-stressed laminated curved panels and cylinders using a wave and finite element method, Journal of Sound and Vibration 332 (7) (2013) 1704 – 1711. doi:/10.1016/j.jsv.2012.09.039.

[31] E. Manconi, B. R. Mace, Estimation of the loss factor of viscoelastic laminated panels from finite element analysis, Journal of Sound and Vibration 329 (19) (2010) 3928 – 3939. doi:/10.1016/j.jsv.2010.04.014.

[32] J.-L. Christen, M. Ichchou, A. Zine, B. Troclet, Wave finite element formulation of the acoustic transmission through complex infinite plates, Acta Acustica united with Acustica 102(6) (2016) 984–991. doi:/10.3813/AAA.919013.

[33] Y. Yang, B. Mace, M. Kingan, Prediction of sound transmission through, and radiation from, panels using a wave and finite element method, J. Acoust. Soc. Am. 141 (4) (2017) 2452–2460. doi:/10.1121/1.4977925.

[34] M. Kingan, Y. Yang, B. Mace, Application of the wave and finite element method to calculate sound transmission through cylindrical structures, Journal of Physics: Conference Series 744. URL http://stacks.iop.org/1742-6596/744/i=1/a=012240

[35] V. Cotoni, R. Langley, P. Shorter, A statistical energy analysis subsystem formulation using finite element and periodic structure theory, Journal of Sound and Vibration 318 (4) (2008) 1077–1108. doi:/10.1016/j.jsv.2008.04.058.

[36] U. Orrenius, H. Liu, A. Wareing, S. Finnveden, V. Cotoni, Wave modelling in predictive vibro-acoustics: Applications to rail vehicles and aircraft, Wave Motion 51 (4) (2014) 635–649. doi:/10.1016/j.wavemoti.2013.11.007.

[37] L. Koval, On sound transmission into an orthotropic shell, Journal of Sound and Vibration 63 (1) (1979) 51–59. doi:/10.1016/0022-460X(79)90376-6.

[38] L. Koval, Sound transmission into a laminated composite cylindrical shell, Journal of Sound and Vibration 71 (4) (1980) 523–530. doi:/10.1016/0022-460X(80)90724-5.

[39] L. Koval, On sound transmission into a thin cylindrical shell under flight conditions, Journal of Sound and Vibration 48 (2) (1976) 265–275. doi:/10.1016/0022-460X(76)90465-X.

[40] B. Liu, L. Feng, A. Nilsson, Sound transmission through curved aircraft panels with stringer and ring frame attachments, Journal of Sound and Vibration 300 (2007) 949–973. doi:/10.1016/j.jsv.2006.09.008.

[41] B. Liu, Noise radiation of aircraft panels subjected to boundary layer pressure fluctuations, Journal of Sound and Vibration 314 (2008) 693–711. doi:/10.1016/j.jsv.2008.01.045.

[42] D. Chronopoulos, B. Troclet, M. Ichchou, J.-P. Laine, A unified approach for the broadband vibroacoustic response of composite shells, Composites Part B: Engineering 43 (2013) 1837–1846. doi:/10.1016/j.compositesb.2012.01.059.

[43] J. Morsbol, S. Sorokin, Elastic wave propagation in curved flexible pipes, International Journal of Solids and Structures 75–76 (2015) 143–155. doi:/10.1016/j.ijsolstr.2015.08.009.

[44] C. Droz, J.-P. Laine, M. Ichchou, G. Inquiete, A reduced formulation for the free-wave propagation analysis in composite structures, Composite Structures 113 (2014) 134–144. doi:/10.1016/j.compstruct.2014.03.017.

[45] A. London, Transmission of Reverberant Sound Through Single Walls, Department of Commerce National Bureau of Standard, Part of the Journal of Research of the National Bureau of Standards 42, Vol. 42, 1949.

[46] Q. Serra, M. Ichchou, J.-F. Deu, Wave properties in poroelastic media using a wave finite element method, Journal of Sound and Vibration 335 (2015) 125–146. doi:/10.1016/j.jsv.2014.09.022.

[47] Q. Serra, M. Ichchou, J.-F. Deu, A wave based condensation method for computing the acoustic efficiency of sound packages submitted to sliding or clamped lateral boundary conditions, International Conference on Noise and Vibration Engineering, ISMA 2014, Leuven.
URL https://hal.archives-ouvertes.fr/hal-01699540

[48] K. Kesour, N. Atalla, A hybrid patch transfer-green functions method to solve transmission loss problems of flat single and double walls with attached sound packages, Journal of Sound and Vibration 429 (2018) 1–17. doi:https://doi.org/10.1016/j.jsv.2018.05.008.
URL http://www.sciencedirect.com/science/article/pii/S0022460X18302827

[49] Acoustics, Measurement of sound insulation in buildings and of building elements using sound intensity – part 1: Laboratory measurements ISO 15186-1:2000, International Standard Organization, Geneva, (2000).

[50] ASTM-International-E2249-02, Standard test method for laboratory measurement of airborne sound transmission loss of building partitions and elements using sound intensity, West Conshohocken (2016).

[51] M. R. Schroeder, The Schroeder frequency revisited, The Journal of the Acoustical Society of America 99 (5) (1996) 3240–3241. doi:/10.1121/1.4148682.